Journal of Solid State Chemistry 183 (2010) 643–648

Contents lists available at ScienceDirect

Journal of Solid State Chemistry

journal homepage: www.elsevier.com/locate/jssc

Enhancement of magnetic ordering temperature in iron substituted ytterbium manganate ($YbMn_{1-x}Fe_xO_3$)

S.L. Samal [a], T. Magdaleno [b], K.V. Ramanujachary [b], S.E. Lofland [c], A.K. Ganguli [a,*]

[a] Department of Chemistry, Indian Institute of Technology, Delhi, Hauz Khas, New Delhi 110016, India
[b] Department of Chemistry and Biochemistry, Rowan University, Glassboro, NJ 08028, USA
[c] Department of Physics and Astronomy, Rowan University, Glassboro, NJ 08028, USA

ARTICLE INFO

Article history:
Received 30 September 2009
Received in revised form
8 January 2010
Accepted 10 January 2010
Available online 18 January 2010

Keywords:
Multiferroics
Rietveld studies
Hexagonal manganites

ABSTRACT

Oxides of the type $YbMn_{1-x}Fe_xO_3$; $x \leq 0.3$ showing multiferroic behavior have been synthesized by the solid state route. These oxides crystallize in the hexagonal structure known for the parent $YbMnO_3$ with the c/a ratio increasing with Fe substitution. The distortion of the MnO_5 polyhedra (tbp) decreases and the Mn–O–Mn bonds in the a–b plane become shorter with Fe-substitution. Magnetic ordering is observed from the low temperature neutron diffraction study. The compounds were found to be antiferromagnetic and the ordering temperature T_N increased from 82 K for pure $YbMnO_3$ to 95 K for $YbMn_{0.7}Fe_{0.3}O_3$. Variable temperature dielectric measurements (15–110 K) show an anomaly in the dielectric constant at temperatures close to the antiferromagnetic ordering temperature for all the compositions, showing a unique correlation between the magnetic and electric field. The increase in the ordering temperature in $YbMn_{1-x}Fe_xO_3$ is explained on the basis of increase in covalence of Mn/Fe–O–Mn/Fe bonds (shorter) with iron substitution.

1. Introduction

Materials with simultaneous presence of more than one ferroic property (multiferroics) with a strong coupling between them have been the subject of tremendous research activity. Control of electric polarization by the application of magnetic field and inducing magnetic ordering by the application of electric field in these materials are expected to lead to next generation multifunctional devices for applications in information storage processes, spintronics, multiple-state memories, magnetoelectric sensors, etc. [1–4]. The rare earth manganites ($RMnO_3$, R=Ho–Lu, Y and Sc) with smaller lanthanides are known for their multiferroic properties with a strong coupling between electric and magnetic dipoles [5–7].

The crystal structure of the hexagonal $RMnO_3$ oxides can be described as made up from corner-linked MnO_5 trigonal bipyramids with free apical oxygen ions. A small tilting of the MnO_5 trigonal bipyramids has been observed along the c axis in this structure [8]. Displacement of R^{3+} ions relative to the oxide layer (formed by the apical oxygen atoms of the MnO_5 bipyramids) and the buckling of the MnO_5 polyhedra have been identified to be responsible for the ferroelectric polarization (ferroelectric Curie temperature T_C=570–990 K) [8,9]. These compounds order antiferromagnetically in the a–b plane at 70–130 K and the detailed magnetic structure of the Mn^{3+} and the R^{3+} (R=Ho, Er, Tm, or Yb) sublattices in these geometrically frustrated hexagonal manganites has been reported earlier [10]. Several efforts have been made to understand the coupling effect between the two ferroic properties [8,11].

For practical applications the magnetically induced polarization has to be accurately tuned by the applied magnetic field and the coupling temperature should be close to room temperature. By suitable magnetic ion substitution the ordering temperature can be varied as is shown by the studies reported here on iron doped $YbMnO_3$. In this class of compounds, the magnetic ordering is driven by the super exchange interactions. The strength of the magnetic interaction depends on the extent of orbital overlap which is dependent on the bond length and bond angle. These structural parameters can be varied by suitable substitution and hence one can tune the magnetic property in these types of materials.

Among the rare-earth manganites, the Yb-analog ($YbMnO_3$), though very interesting, has been less studied [6,12–15]. Fujimura et al. [12] reported magnetic field-induced ferromagnetism in ferroelectric $YbMnO_3$ epitaxial films. Magnetization measurements of $YbMnO_3$ showed an antiferromagnetic transition at T_N=82 K, where only the Yb^{3+} ion has a localized 4f moment [6]. From the neutron studies it has been observed that the magnetic structure of $YbMnO_3$ is considerably diverse than the $YMnO_3$ and also the Mn order is affected by the type of rare-earth substitution

* Corresponding author. Fax: +91 11 26854715.
E-mail addresses: ashok@chemistry.iitd.ernet.in, ashok@chemistry.iitd.ac.in (A.K. Ganguli).

0022-4596/$ - see front matter © 2010 Elsevier Inc. All rights reserved.
doi:10.1016/j.jssc.2010.01.007

[16]. Moreover the behavior of the Yb ions in $YbMnO_3$ at two sites (Rare earth has two different crystallographic sites in hexagonal structure) are different. The Yb ions at 4*b* site are polarized by the exchange interaction with Mn^{3+} below T_N, whereas no such effect has been observed for Yb at 2*a* site. So the strength of magnetic exchange interaction in $YbMnO_3$ is in the order of Mn–Mn > Yb–Mn > Yb–Yb [16].

There has been no report so far (to the best of our knowledge) on iron substituted $YbMnO_3$. We have synthesized the Fe-doped oxides, $YbMn_{1-x}Fe_xO_3$ ($x \leq 0.3$) for the first time and report the presence of magneto-electric coupling in all the compounds, indicative of multiferroic behavior. The increase in magnetic ordering temperature with Fe content corresponds with the increase in covalence character of Mn/Fe–O–Mn/Fe bond.

2. Experimental

Polycrystalline samples of $YbMn_{1-x}Fe_xO_3$ (x=0.0, 0.1, 0.2, 0.3) were synthesized by mixing stoichiometric amounts of Yb_2O_3 (Aldrich, 99.9%), Mn_2O_3 (Aldrich, 99.9%) and Fe_2O_3 (Aldrich, 99.9%). Yb_2O_3 was preheated at 900 °C before weighing. All the oxides were mixed and ground in an agate mortar to obtain a homogeneous mixture. The mixtures were then loaded in a ceramic boat and heated at 950 °C for 12 h. The mixture was then ground and further calcined at 1100 °C for 20–30 h in air which enabled the formation of the desired oxides. The powder was ground, pressed into disks of 10 mm diameter and ~1 mm thickness under a pressure of 1.5 GPa. The disks were sintered in air at 1150 °C for 15 h for the dielectric measurements.

All the above compounds were characterized by a Bruker D8 Advance Powder Diffractometer using Cu$K\alpha$ radiation. X-ray data for Rietveld refinement was collected in the 2θ range of 10–90°. A step size of 0.01° and a step time of 6 s per step were used. Rietveld refinement of X-ray diffraction data were carried out with GSAS software [17]. The background was modeled by a shifted Chebyschev polynomial of the first kind with 10 variables, and the peak profile was simulated with the pseudo-Voigt function.

Neutron diffraction data at RT and low temperature were collected at the Dhruva reactor, beam port T1013, Trombay, India. The instrument is a five-position sensitive-detector-based powder diffractometer (λ=1.249 Å) with $\Delta d/d$=0.8%. For low-temperature experiments, the powder sample was packed in a vanadium can of height 60 mm and diameter 4 mm. The data were collected in the 2θ range from 10° to 90° with a step size of 0.05°. Low-temperature diffraction data were achieved using a closed cycle helium refrigerator. The lowest achievable temperature was 17 K.

The density of the sintered disks was measured by the Archimedes method and was found to be in the range of 87–90% of the theoretical density. Low-temperature dielectric measurements were carried out using a Quad Tech 1920 LCR precision meter and a cryogen-free low-temperature high magnetic field system on sintered disks coated with silver. The dielectric measurements were repeated twice to check the reproducibility of the data. The polarization–electric field (P–E) hysteresis loop was obtained using a Sawyer–Tower circuit and a ferroelectric test system (Trek 609B; Precision Premier II, Radiant Technologies Inc.). Magnetic data were collected on a Quantum Design, Physical Property Measuring System vibrating sample magnetometer between 5 and 300 K. Data were collected during both the cooling and the warming cycles at an applied magnetic field of 0.5 T. Room temperature optical absorption spectra were recorded in the 1100–200 nm wavelength range with a Perkin–Elmer Lambda Bio 20 UV–vis–NIR spectrophotometer.

3. Results and discussion

X-ray diffraction studies of the samples heated at 1100 °C show monophasic oxides of the type $YbMn_{1-x}Fe_xO_3$ ($0.0 \leq x \leq 0.3$) (Fig. 1). All the reflections could be satisfactorily indexed to a hexagonal cell. The samples were dark green in color and highly resistive. The variation of lattice parameters with iron doping is shown in Fig. 2. The ***a*** lattice parameter decreases, whereas the ***c*** lattice parameter increases with iron content. The increase in ***c*** lattice parameter could be due to increase in d_z^2 population in the trigonal bipyramidal (TBP) geometry. Similar observation on the lattice parameter variation has been reported earlier for the analogous yttrium series, $YMn_{1-x}Fe_xO_3$ in the regime of $0.2 \leq x \leq 0.3$ [18]. It may be noted that in the range of $0.0 \leq x \leq 0.2$, $YbMn_{1-x}Fe_xO_3$ show opposite trend than is observed for $YMn_{1-x}Fe_xO_3$. We observed a decrease in a lattice parameter with x in $YbMn_{1-x}Fe_xO_3$ though the given ionic radii data for Mn^{3+} and Fe^{3+} are same (0.58 Å) in fivefold coordination [19].

Rietveld refinement studies of X-ray diffraction data were carried out for all the compositions. The occupancies of iron and manganese were kept fixed to the loaded composition due to the small electron density difference between the two. All the atomic positions, structural and isotropic thermal parameters (B_{iso}) were refined. The final refined positional and thermal parameters are

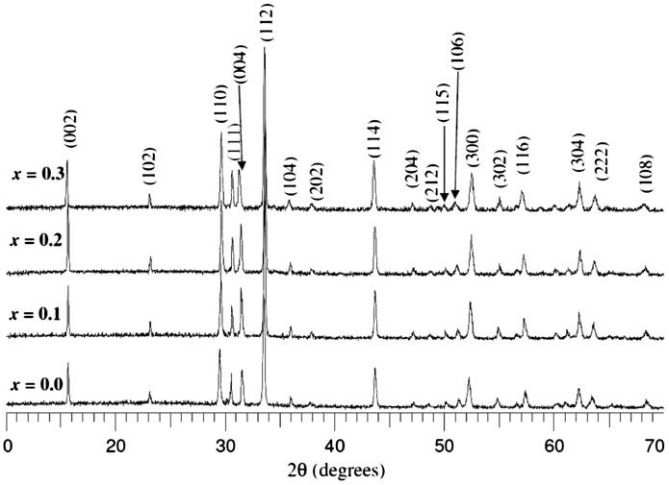

Fig. 1. Powder X-ray diffraction patterns of $YbMn_{1-x}Fe_xO_3$ ($0 \leq x \leq 0.3$).

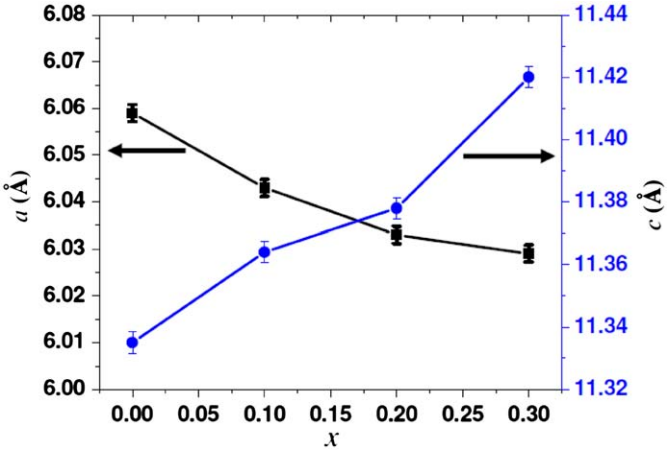

Fig. 2. The variation of a- and c-lattice parameters as a function of x.

given in Table 1. Some selected bond distances and bond angle is given in Table 2. The Mn–O3 and Mn–O4 bond lengths decrease, whereas the Mn–O1 and Mn–O2 bond length increase with iron content.

Thermogravimetric analysis was carried out in H_2 and N_2 atmosphere to ascertain the oxygen stoichiometry of $YbMn_{1-x}Fe_xO_3$ compounds. Calculation of the oxygen content was carried out assuming Mn^{3+} to be reduced to Mn^{2+} and Fe^{3+} to Fe metal in H_2/N_2 atmosphere. For all the compounds except $x=0.3$, the oxygen content was found to be in excess of 3 (Table 3). The excess oxygen could be accounted for the partial reduction of Yb^{3+} to Yb^{2+} in hydrogen environment and at high temperature [20]. The lower oxygen content for the $x=0.3$ phase might be due to the presence of some impurity. However, we did not observe any impurity phase from powder X-ray diffraction data.

Table 1
Rietveld refinement data of $YbMn_{1-x}Fe_xO_3$, $x=0.0$, 0.1, 0.2 and 0.3.

		$YbMnO_3$	$YbMn_{0.9}Fe_{0.1}O_3$	$YbMn_{0.8}Fe_{0.2}O_3$	$YbMn_{0.7}Fe_{0.3}O_3$
a (Å)		6.0701(1)	6.0582(1)	6.0496(1)	6.0472(1)
c (Å)		11.3567(2)	11.3758(2)	11.4132(2)	11.4575(2)
V (Å^3)		362.39(1)	361.57(1)	361.74(1)	362.85(1)
Atoms					
Yb(1)	z	0.2689(2)	0.2679(3)	0.2584(3)	0.2585(2)
	B_{iso}(Å^2)	0.71(4)	0.52(3)	0.65(2)	0.48(2)
Yb(2)	z	0.2280(2)	0.2274(3)	0.2188(5)	0.2196(2)
	B_{iso}(Å^2)	0.52(3)	0.63(4)	0.53(4)	0.48(2)
Mn	x	0.3248(10)	0.3307(12)	0.3259(14)	0.3215(13)
	z	0.0	0.0	−0.0011(4)	−0.0012(5)
	n	1.0	0.9	0.8	0.7
	B_{iso}(Å^2)	0.92(8)	0.74(4)	0.83(5)	0.71(7)
Fe	x	–	0.3307(12)	0.3259(14)	0.3167(13)
	z	–	0.0	−0.0011	−0.0012(5)
	n	0.0	0.1	0.2	0.3
	B_{iso}(Å^2)	–	0.74(4)	0.83(5)	0.71(7)
O(1)	x	0.3164(21)	0.3121(18)	0.3108(19)	0.3095(22)
	z	0.1618(11)	0.1619(12)	0.1612(11)	0.1615(13)
	B_{iso}(Å^2)	3.1(2)	2.45(9)	2.53(8)	2.3(3)
O(2)	x	0.6721(26)	0.6489(23)	0.6412(21)	0.6391(22)
	z	0.3365(9)	0.3361(8)	0.3359(7)	0.3362(9)
	B_{iso}(Å^2)	2.8(3)	2.24(7)	2.63(9)	2.7(2)
O(3)	z	0.4761(12)	0.4885(20)	0.4968(18)	0.4998(17)
	B_{iso}(Å^2)	1.61(8)	2.05(9)	1.73(7)	2.11(9)
O(4)	z	0.0313(18)	0.0147(21)	0.0098(11)	0.0068(10)
	B_{iso}(Å^2)	2.4(5)	2.35(11)	2.71(9)	2.06(12)
	R_p (%)	6.41	6.25	6.16	5.97
	R_{wp} (%)	8.31	8.57	8.65	8.03
	χ^2	2.68	3.14	3.26	2.86

Crystal system: hexagonal; space group: $P6_3cm$.

Table 2
Selected bond distances and bond angles for $YbMn_{1-x}Fe_xO_3$, $x=0.0$, 0.1, 0.2 and 0.3.

Atoms	$YbMnO_3$ (Å)	$YbMn_{0.9}Fe_{0.1}O_3$ (Å)	$YbMn_{0.8}Fe_{0.2}O_3$ (Å)	$YbMn_{0.7}Fe_{0.3}O_3$ (Å)
Mn–O1	1.843(3)	1.845(3)	1.866(4)	1.869(2)
Mn–O2	1.867(3)	1.871(3)	1.874(4)	1.878(2)
Mn–O3	2.059(2)	2.061(2)	2.057(3)	2.052(1)
Mn–O4	1.988(2)	1.958(5)	1.901(4)	1.903(2)
〈Mn–O〉	1.963(12)	1.958(15)	1.951(18)	1.950(8)
Yb1–O1	2.419(2)	2.415(2)	2.3621(3)	2.342(1)
Yb1–O2	2.094(2)	2.092(2)	2.1340(2)	2.095(3)
Yb1–O3	2.439(4)	2.546(5)	2.6408(6)	2.635(4)
Yb2–O1	2.022(2)	2.019(2)	1.9840(2)	1.967(3)
Yb2–O2	2.520(2)	2.516(2)	2.5655(3)	2.524(3)
Yb2–O4	2.326(4)	2.357(4)	2.4178(5)	2.421(6)
Angle (deg)				
O1–Mn–O2	177.99(2)	178.71(3)	178.82(3)	179.12(1)
O1–Mn–O3	98.35(4)	95.46(2)	92.84	90.78
O1–Mn–O4	78.18(2)	81.73(3)	85.52	86.42
O2–Mn–O3	82.17	84.39(5)	84.79	82.49
O3–Mn–O3	116.67(5)	116.15(8)	114.13(15)	114.08
O3–Mn–O4	121.62(4)	121.91(6)	122.51(23)	122.94
Mn–O3–Mn	119.13(12)	119.79(10)	119.27(21)	119.76
Mn–O4–Mn	118.39(8)	118.65(9)	119.21(18)	119.75

Table 3
Details of oxygen content, magnetic moment and Weiss constant of $YbMn_{1-x}Fe_xO_3$.

Composition	Oxygen content	Weiss constant (K)	μ_{exp} (B.M)	μ_{theor} (B.M)	T_N (K)	T_ε (K)
$YbMnO_3$	3.19	−166	6.40	6.68	82	85
$YbMn_{0.9}Fe_{0.1}O_3$	3.17	−168	6.71	6.76	87	90
$YbMn_{0.8}Fe_{0.2}O_3$	3.22	−172	7.57	6.84	92	93
$YbMn_{0.7}Fe_{0.3}O_3$	2.86	−183	8.11	6.92	95	98

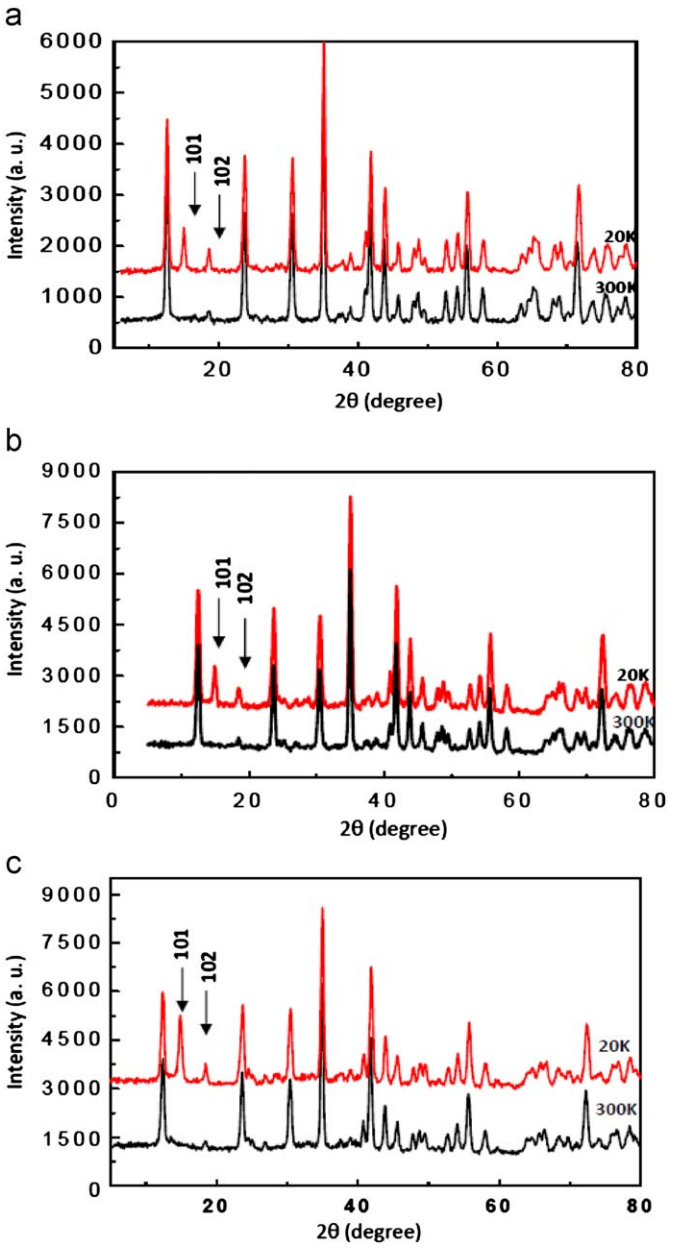

Fig. 3. Neutron diffraction pattern of $YbMn_{1-x}Fe_xO_3$: (a) x=0.0, (b) x=0.1 and (c) x=0.2 at 20 and 300 K. The arrows with Miller indices refer to magnetic Bragg peaks.

Neutron diffraction study of $YbMn_{1-x}Fe_xO_3$ (x=0, 0.1, 0.2) show (Fig. 3) appearance of magnetic Bragg peaks at low temperature (20 K), indicative of magnetic ordering with 120° structure for all the compositions. The (101) peak appears due to the ordering of Mn ions [16] and the (102) Bragg peak involves the contribution from both Mn and Yb ordering. A relatively strong peak is observed for x=0.2, which indicates a stronger magnetic

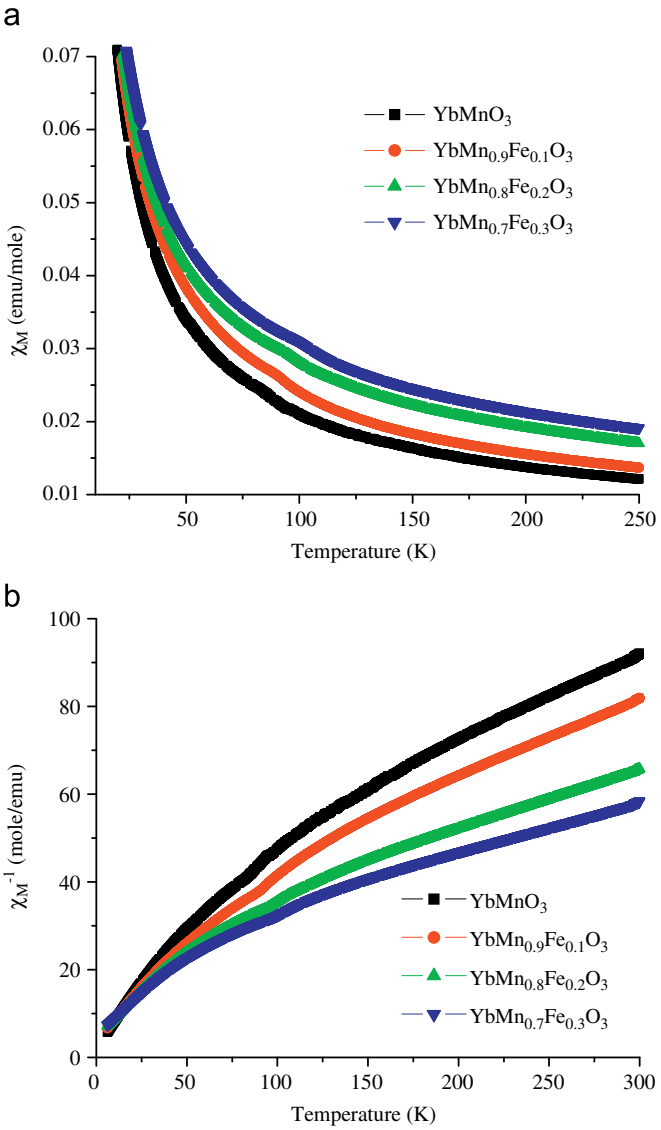

Fig. 4. Temperature variation of (a) molar magnetic susceptibility (χ_M) and (b) the inverse molar magnetic susceptibility of $YbMn_{1-x}Fe_xO_3$ at an applied field of 5 kOe.

exchange interaction. It may be noted that in $YMnO_3$, the Mn order does not induce a strong (101) magnetic peak [21]. This clearly indicates that the magnetic order is affected by different rare earth substitution.

Fig. 4 shows the temperature variation of the magnetic susceptibility plots of $YbMn_{1-x}Fe_xO_3$ (x=0.0, 0.1, 0.2 and 0.3). Although no clear magnetic transition is observed in the $YbMn_{1-x}Fe_xO_3$ samples, all show a kink in the temperature range of 82–95 K [Fig. 4(a)], indicative of antiferromagnetic ordering and the ordering temperature increases with iron content. The negative Weiss temperature (θ) indicates antiferromagnetic interactions and the magnitude increases

with Fe content (Table 3). The theoretical magnetic moments μ_{theor} were calculated by assuming both Mn and Fe to be in the trivalent state and taking into account the contribution of the Yb ion. The experimental values (μ_{exp}), determined from the high temperature region of the inverse susceptibility plot, match reasonably with the theoretical estimates, especially since it is well known that the rare earth ions order at much lower temperature than the transition metal ions [22]. For instance, the ordering temperature for the Er sublattice in $ErMnO_3$ occurs below 10 K while the Mn network orders at 80 K [23].

Fig. 5 shows the *P*–*E* hysteresis loops for $YbMn_{1-x}Fe_xO_3$ with x=0.0 and 0.1 at 300 K. Ferroelectric behavior has been observed for all the compositions. However, with increasing Fe content, the compound becomes more lossy, and the ferroelectric behavior becomes weaker. Filippetti et al. studied the role of *d*-electron occupancy on the *c*-axis electric polarization in hexagonal manganites [24]. The *d* orbitals oriented in the direction of the ferroelectric distortion have to be formally empty. In $YbMnO_3$, the four *d* orbitals (d_{xz}, d_{yz}, d_{xy} and $d_{x^2-y^2}$) are filled and only the d_z^2 orbital is empty. Thus, the d_z^2 orbital can be actively involved in hybridization with the oxygen p_z orbital. This eventually induces a ferroelectric distortion along the *c* axis in hexagonal manganites. It may be rationalized that substituting Fe^{3+} (a d^5 ion) in $YbMnO_3$ leads to an increase in occupancy of the d_z^2 orbital which lowers the degree of hybridization between Mn d_z^2 and O p_z orbitals. This could then explain the weakening of ferroelectricity with Fe substitution and increase in the lossy nature of the $Yb(Mn/Fe)O_3$ compounds.

The dielectric constant (ε) and loss ($\tan\delta$) of the above oxides were also measured at low temperatures (Fig. 6). The dielectric loss is very low (within the experimental error) at temperatures below 130 K. Anomalies in 'ε' at temperatures close to the antiferromagnetic ordering temperature occur in all the compounds, which indicates a unique correlation between the magnetic and electric dipoles in these compounds. The temperature of dielectric anomaly increases with increase in Fe content (Table 3) which corroborates with the magnetic ordering.

From both magnetic and low-temperature dielectric study of $YbMn_{1-x}Fe_xO_3$, we observed an increase in the ordering temperature with iron substitution (Table 3). It is known that the magnetic ordering temperature of $ScMnO_3$ (129 K) is higher than that of $YMnO_3$ (70 K) [21]. This has been explained on the basis of shorter Mn–O bond distances observed in $ScMnO_3$ compared to $YMnO_3$, which effectively lead to strong exchange interactions and higher ordering temperature for $ScMnO_3$ related to $YMnO_3$. In the $RMnO_3$ compounds the magnetic interactions among the Mn atoms are through super-exchange interactions via Mn–O–Mn bonds in the *a*–*b* plane. In the series of compounds discussed here ($YbMn_{1-x}Fe_xO_3$), a higher electronegative ion (Fe^{3+}, 1.9) is substituted in place of Mn^{3+}, (electronegativity of 1.55) [25]. This indeed leads to the increase in the covalence of Mn–O–Mn bonds. It is well known that the magnetic interaction strength depends on the extent of the orbital overlap and hence covalence of the bond [26]. Further, from the Rietveld refinement study (Table 2) it is observed that the bond distance between the manganese and oxygen atoms present in the equatorial plane (O3, O4) shortens with increase in iron content. The decrease in bond length leads to increase in the extent of orbital overlap. This increases the covalence of (Fe/Mn)–O bonds and hence stronger exchange interaction. It may be noted that the ***a*** lattice parameter decreases with Fe content and the magnetic interaction occurs in the ***a***–***b***

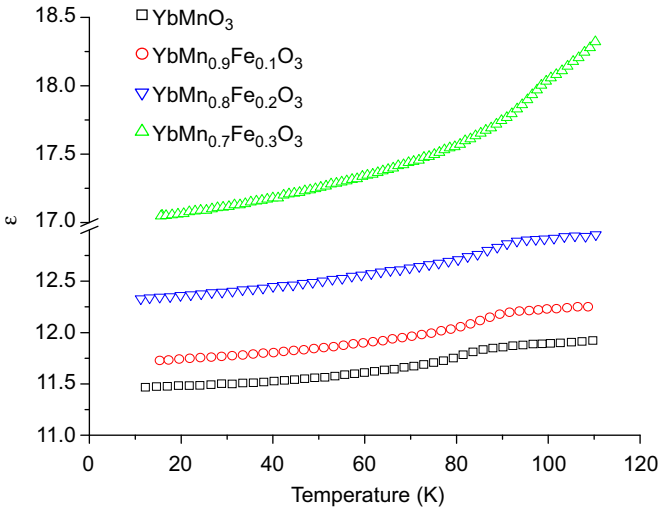

Fig. 6. Low-temperature dielectric constant measurements of $YbMn_{1-x}Fe_xO_3$; x=0.0, 0.1, 0.2, and 0.3.

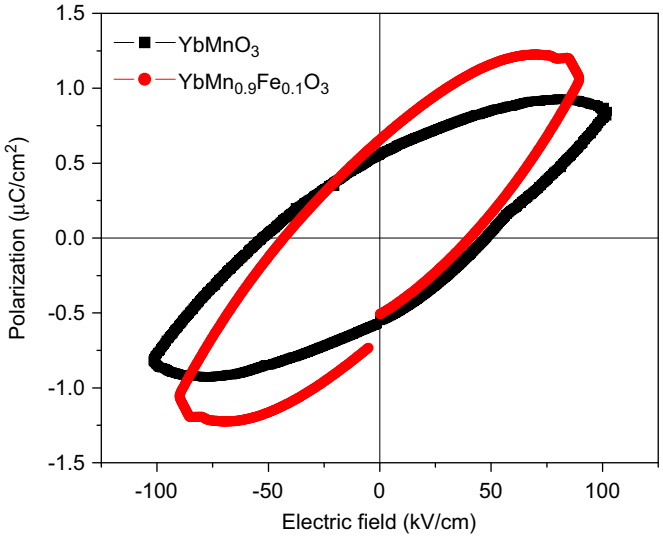

Fig. 5. Polarization versus electric field loop of $YbMn_{1-x}Fe_xO_3$; x=0.0 and 0.1 at room temperature.

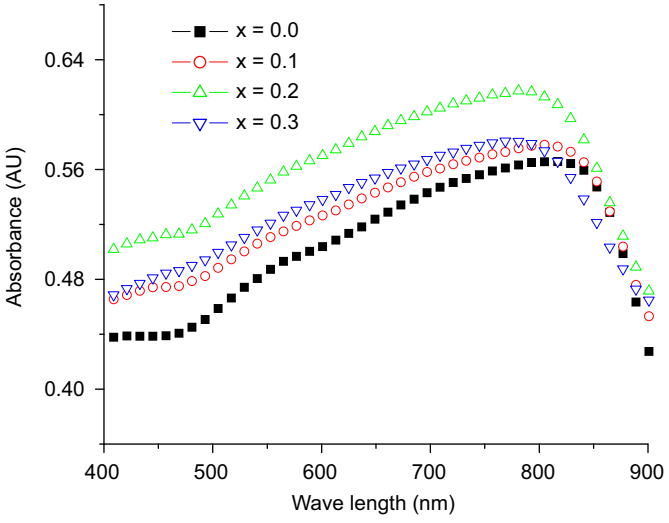

Fig. 7. Absorption spectra for $YbMn_{1-x}Fe_xO_3$ ($0.0 \le x \le 0.3$).

Table 4
Band gap of $YbMn_{1-x}Fe_xO_3$ determined from absorption study.

Composition	Band gap (nm)
$YbMnO_3$	849
$YbMn_{0.9}Fe_{0.1}O_3$	837
$YbMn_{0.8}Fe_{0.2}O_3$	815
$YbMn_{0.7}Fe_{0.3}O_3$	799

plane of the hexagonal manganites. So the increase in covalence of (Fe/Mn)–O accounts for both the increase in magnetic ordering temperature and the decrease in the ***a*** lattice parameter (with iron content) in $YbMn_{1-x}Fe_xO_3$. On increasing the concentration of Fe, there are more Fe–Fe nearest neighbors, leading to a larger average antiferromagnetic interaction. Since the magnetic interaction occurs in the ***a***–***b*** plane of the hexagonal manganites, so the increase in $|\theta|$ with decreasing ***a*** is qualitatively consistent with increase in magnetic interactions originating from the shortening of the ***a*** parameter.

Typical room temperature optical absorption spectra for $YbMn_{1-x}Fe_xO$ samples are shown in Fig. 7. It is observed that the band gap increases with Fe concentration (Table 4). In hexagonal manganites, the top of the valence band has a predominantly Mn $3d_{x^2-y^2}-O\ 2p_{x,y}$ character and the lowest unoccupied band has Mn $3d_z^2-O\ 2p_z$ character [27]. By substituting a more electronegative ion (Fe^{3+}) the energy level of the top of the valence band decreases, which can explain the increase in the band gap in $YbMn_{1-x}Fe_xO_3$ with increase in iron content.

4. Conclusions

Pure hexagonal phases of the type $YbMn_{1-x}Fe_xO_3$ ($0.0 \le x \le 0.3$) have been synthesized by solid state method. All the compounds show magneto-electric effect in the range of 82–95 K. *P*–*E* measurement shows compounds are ferroelectric in nature and compounds with higher Fe content are more lossy. Both magnetic ordering temperature and the temperature of dielectric anomaly increase with Fe content which is encouraging. Hexagonal $RMnO_3$ based oxides are antiferromagnetic with spin frustration, so any change in the crystal structure leads to a change in the magnetic properties. We have found that by varying the electronegativities of the transition metal one can alter the magnetic ordering temperature. These studies help to understand the structure–property relationship in hexagonal $RMnO_3$ type multiferroics.

Acknowledgment

The authors thank Dr S. Patnaik and Mr Anil Kumar of JNU, New Delhi for the low temperature dielectric measurements and Dr S.M. Yusuf, BARC, Mumbai for the neutron diffraction study. S.L.S. would like to thank CSIR for a research fellowship. A K.G. thanks DST and BRNS for funding. S.E.L. acknowledges support from NSF MRSEC DMR 0520471. KVR acknowledges the support of CP-STIO program of DST, Government of India.

References

[1] M. Fiebig, J. Phys. D 38 (2005) R123–R152.
[2] W. Prellier, M.P. Singh, P. Murugavel, J. Phys. Condens. Matter 17 (2005) R803–R832.
[3] N.A. Spaldin, M. Fiebig, Science 309 (2005) 391–392.
[4] X. Qi, J. Dho, R. Tomov, M.G. Blamire, J.L. MacManus-Driscoll, Appl. Phys. Lett. 86 (2005) 062903(1)–062903(3).
[5] Z.J. Huang, Y. Cao, Y.Y. Sun, Y.Y. Xue, C.W. Chu, Phys. Rev. B 56 (1997) 2623–2626.
[6] T. Katsufuji, S. Mori, M. Masaki, Y. Moritomo, N. Yamamoto, H. Takagi, Phys. Rev. B 64 (2001) 104419(1)–104419(6).
[7] M. Fiebig, Th. Lottermoser, D. Frohlich, A.V. Goltsev, R.V. Pisarev, Nature 419 (2002) 818–820.
[8] B.B. Van Aken, T.T.M. Palstra, A. Filippetti, N.A. Spaldin, Nat. Mater. 3 (2004) 164–170.
[9] Th. Lonkai, D.G. Tomuta, U. Amann, J. Ihringer, R.W.A. Hendrikx, D.M. Tobbens, J.A. Mydosh, Phys. Rev. B 69 (2004) 134108(1)–134108(10).
[10] M. Fiebig, Th. Lottermoser, R.V. Pisarev, J. Appl. Phys. 93 (2003) 8194–8196.
[11] S.-W. Cheong, M. Mostovoy, Nat. Mater. 6 (2007) 13–20.
[12] N. Fujimura, T. Takahashi, T. Yoshimura, A. Ashida, J. Appl. Phys. 101 (2007) 09M107(1)–09M107(3).
[13] K. Yoshii, H. Abe, J. Solid State Chem. 165 (2002) 131–135.
[14] M. Fiebig, N.P. Duong, T. Satoh, Th. Lottermoser, J. Magn. Magn. Mater. 300 (2006) e264–e269.
[15] T. Takahashi, T. Yoshimura, N. Fujimura, Jpn. J. App. Phys. 45 (2006) 7329–7331.
[16] X. Fabreges, I. Mirebeau, P. Bonville, S. Petit, G. Lebras-Jasmin, A. Forget, G. Andre, S. Pailhes, Phys. Rev. B 78 (2008) 214422.
[17] A.C. Larson, R.B. Von Dreele, General Structure Analysis System (GSAS), Los Alamos National Laboratory Report LAUR 2004, 86–748.
[18] S.L. Samal, W. Green, S.E. Lofland, K.V. Ramanujachary, D. Das, A.K. Ganguli, J. Solid State Chem. 181 (2008) 61–66.
[19] R.D. Shannon, Acta Crystallogr. A 32 (1976) 751–767.
[20] S.M. Kaczmarek, T. Tsuboi, M. Ito, G. Boulon, G. Leniec, J. Phys. Condens. Matter 17 (2005) 3771–3786.
[21] A. Munoz, J.A. Alonso, M.J. Martinez-Lope, M.T. Casais, J.L. Martinez, M.T. Fernandez-Diaz, Phys. Rev. B 62 (2000) 9498–9510.
[22] N. Iwata, K. Kohn, J. Phys. Soc. Jpn. 67 (1998) 3318–3319.
[23] J. Park, U. Kong, S.I. Choi, J.-G. Park, C. Lee, W. Jo, Appl. Phys. A 74 (2002) S802–S804.
[24] A. Filippetti, N.A. Hill, Phys. Rev. B 65 (2002) 195120(1)–195120(11).
[25] L. Pauling, in: The nature of the chemical bond and the structure of molecules and crystals: an introduction to modern structural chemistry, third ed., Cornell University Press, New York, 1960, p. 93 (Chapter 3).
[26] J.B. Goodenough, in: Magnetism and the Chemical Bond, Interscience Publishers, Wiley, New York, London, 1963, pp. 75–81.
[27] J.E. Medvedeva, V.I. Anisimov, M.A. Korotin, O.N. Mryasov, A.J. Freeman, J. Phys. Condens. Matter 12 (2000) 4947–4958.